O'Brien, H. M., Manzotti, M., Abrams, R. D., Elorriaga, D., Sparkes, H. A., Davis, S. A., & Bedford, R. B. (2018). Iron-catalysed substrate-directed Suzuki biaryl cross-coupling. *Nature Catalysis*, *1*(6), 429-437. https://doi.org/10.1038/s41929-018-0081-x

Iron-catalysed substrate-directed Suzuki biaryl cross-coupling.

Harry M. O'Brien, Mattia Manzotti, Roman D. Abrams, David Elorriaga, Hazel A. Sparkes, Sean A. Davis, Robin B. Bedford*.

School of Chemistry, University of Bristol, Cantock's Close, Bristol, BS8 1TS, UK. Email: r.bedford@bristol.ac.uk

Abstract: Although the replacement of ubiquitous palladium catalysts with more sustainable iron-based analogues continues apace, the simple biaryl Suzuki cross-coupling reaction remains stubbornly elusive. It appears that the main issue hampering the reaction is activation of the aryl halide C-X bond. Here we show that simple *N*-pyrrole amide and related directing groups on the aryl halide substrates facilitate this process by transient π-coordination to the iron centre. This allows iron-catalysed Suzuki biaryl cross-coupling to proceed, with alkyllithium-activated aryl pinacol boronic esters, under mild conditions.

The palladium-catalysed Suzuki biaryl cross-coupling reaction (Figure 1(a); M = Pd) is a powerful and very widely used method for the construction of new biaryl motifs.[1,2] It is exploited in the synthesis of a range of commercial products including the intermediate OTBN, used in the production of six different Sartan-class drugs for the treatment of hypertension, and it is employed by BASF in the production of the broad-spectrum fungicide, Boscalid.[3] While palladium-based catalysts are ubiquitous in the Suzuki reaction, palladium is expensive, scarce and its extraction environmentally deleterious. Furthermore, as with all platinum group metals, there are strict regulatory requirements to remove Pd to the low ppm levels in active pharmaceutical intermediates.[4] Therefore, there is a growing impetus to replace palladium catalysts with more sustainable counterparts based on Earth-abundant metals, with the first-row transition metals being particularly appealing candidates. Significant progress has been made with nickel-[5-10] and copper-catalysed[11-14] Suzuki biaryl coupling, while promising results have recently been obtained with cobalt.[15-17]

Iron is especially attractive as a potential replacement for palladium due the metal's very low cost, wide availability and comparatively low toxicity, and is increasingly being employed in a

range of cross-coupling reactions.[18-20] Furthermore, a good deal of success has already been enjoyed in the coupling of arylboron reagents of the form $ArBR_3^-$ and $ArRB(pin)^-$ (pin = pinacolato, **1**) with alkyl, benzyl, allyl and 2-heteroaryl halides, in the presence of co-catalytic Zn or Mg salts.[21-26] However, the iron-catalysed Suzuki *biaryl* cross-coupling reaction (Figure 1(a); M = Fe) remains problematic,[27] with early reports proving unreproducible,[28,29] leading to subsequent retractions. Indeed, to the best of our knowledge, the only example of a Suzuki biaryl cross-coupling reaction that occurs under mild conditions[30] is obtained in the coupling of 2-halobenzyl halides with the activated boronic ester **1a**, which gives the expected benzyl-arylated product **2** along with some of the biaryl coupled-side product **3**.[31] We speculated that the biaryl bond-formation in this case may be due to the substrate 'directing' the activation of the aryl-X bond at the iron centre, as has been observed previously in the olefin-assisted alkylation of aryl chlorides.[32] However, aryl halides with classic *ortho*-directing groups based on tertiary amine, ether, ester, carbamate or imine functions all failed to give the desired cross-coupling.[31]

We now report our preliminary findings into the arylation of aryl chloride substrates with *N*-pyrrole amide and related directing groups (**4**, Figure 1(d)), which demonstrate unequivocally that iron-catalysed Suzuki biaryl bond-formation is an attainable goal.

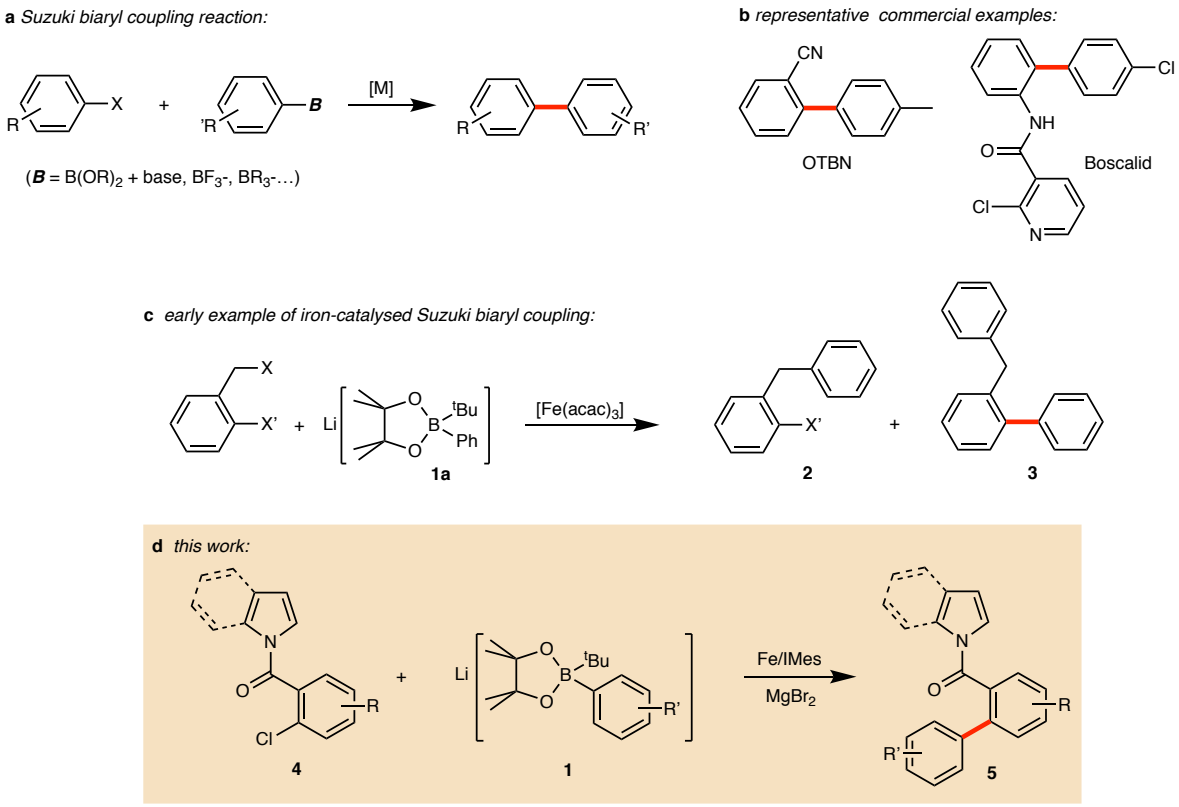

Figure 1. Suzuki biaryl cross-coupling reactions. a, The Suzuki biaryl cross-coupling reaction. **b**, Selected commercial examples. **c** and **d**, Directing group approaches to iron catalysed Suzuki biaryl cross-coupling.

Results

Optimisation studies.

Table 1 summarises part of the optimisation studies undertaken for the coupling of the *N*-pyrrole amide-based aryl chloride **4a** with the activated organoborate **1a** (for full details see Supplementary Methods and Supplementary Table 1). The use of $FeBr_3$ in the absence of added ligands gave poor activity (entry 1) as did the use of $FeBr_3$ with amine or phosphine ligands (Supplementary Table 1). By contrast, *N*-heterocyclic carbene (NHC) ligands proved to be beneficial, depending critically on the substitution pattern of the *N*-aryl groups. The general trend appears to be that modest steric bulk in the 2- and 6-positions gave improved performance, but that overly encumbered substituents in these positions were highly deleterious (Table 1, entries 2 and 3). The best activity was seen with IMes, at 60 °C (entry 9), while removing the *o*-Me groups led to a decreased yield (entry 8). The use of $FeBr_2$ in place of $FeBr_3$ gave identical performance (entry 10), importantly, high-purity iron(II) bromide gave slightly improved performance (entry 11),[27] while no reaction was observed in absence of iron

(entry 12). This indicates that impurities, in either the iron source or one of the other components of the reaction mixture, are unlikely to be responsible for the observed catalytic activity. A similar result was obtained on employing high-purity iron chloride (see Supplementary Table 1). Slightly improved performance was obtained when the **IMes** : Fe ratio was reduced from 2 : 1 to 1 : 1 (Table 1, entry 13). While reducing the equivalents of boronate **1a** to 2.2 with respect to **4a** had no impact on productivity (entry 14), lower loadings proved deleterious (Supplementary Table 1). In all cases, we employed the pre-formed boronate **1a**, although a similar performance was seen on preparing **1a** *in situ* from phenyl boronic pinacol ester and ^{t}BuLi (entry 15). The boronate **1a** was readily formed in 85% yield on a 30 g scale, and its crystal structure is shown in Figure 2(a). Meanwhile, the crystal structure of **5a** was also obtained and is shown in Figure 2(b), confirming the identity of the coupled product. Free IMes gave similar performance (entry 16) to the far more easily handled **IMes·HCl** precursor, for this reason the salt was employed for most subsequent catalysis.

Table 1. Optimisation studies.

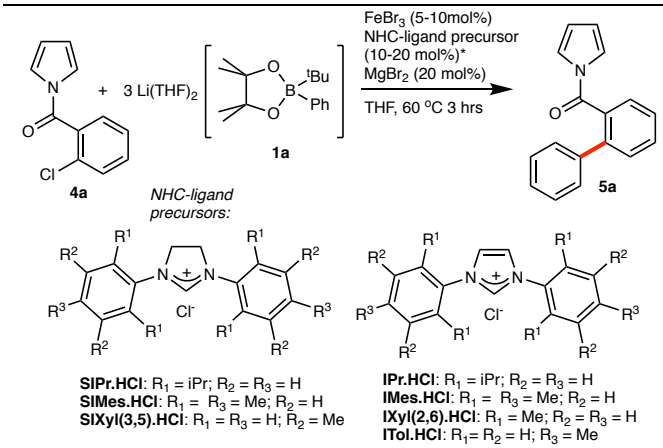

Entry	Amount $FeBr_3$ (mol%)	NHC-ligand precursor (mol%)	Temp., °C	Yield, %
1	10	none	r.t.	16
2	10	**SIPr·HCl** (20)	r.t.	3
3	10	**IPr·HCl** (20)	r.t.	0
4	10	**SIMes·HCl** (20)	r.t.	22
5	10	**IMes·HCl** (20)	r.t.	27

6	10	**IXyl(2,6)·HCl** (20)	60	67
7	10	**SIXyl(3,5)·HCl** (20)	60	29
8	10	**ITol·HCl** (20)	60	24
9	10	**IMes·HCl** (20)	60	73
10[†]	10	**IMes·HCl** (20)	60	73
11[‡]	10	**IMes·HCl** (20)	60	84
12	none	**IMes·HCl** (10)	60	0
13	10	**IMes·HCl** (10)	60	82
14[¶]	10	**IMes·HCl** (10)	60	82
15[ß]	10	**IMes·HCl** (10)	60	81
16	10	**IMes** (10)	60	80

Yields determined by GC analysis (dodecane internal standard). *$FeBr_3$ and NHC precursor stirred at room temperature for 1 hour prior to addition of other reaction components. [†]$FeBr_2$ used in place of $FeBr_3$. [‡]Reaction using 99.999% $FeBr_2$, stirred with NHC precursor at 60 °C for 30 mins prior to addition of other reaction components. [¶]Reaction using 2.2 equivalents of **1a**. [ß]Reaction using **1a** formed *in situ*. See Supplementary Information for experimental details.

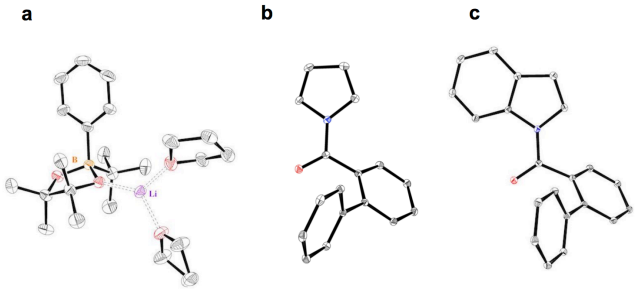

Figure 2. **Single crystal X-ray structures**. **a**, The activated pinacol boronic ester, **1a. b** and **c** The Suzuki-coupled products **5a** and **5b** respectively. Thermal ellipsoids set at 30% probability, H-atoms omitted for clarity. See Supplementary Table 3 and Supplementary Figures 13–15 for crystallographic details.

The effects of changing either: (i) the type and position of the halide or (ii) the amido-based directing group are summarised in Figure 3. The 2-bromo analogue (**4b**), showed reduced but reasonable conversion to the desired product **5a** compared to the chloride counterpart, but this was accompanied by a significant rise in the amount of hydrodehalogenated side-product, **6**. This species became the main product when the iodide-containing substrate **4c** was used. Meanwhile, the 2-fluoro substrate **4d** showed poor conversion to the desired

product, but essentially no hydrodehalogenation. It is clear the 2-chloro function represents the best balance of activity and selectivity, and was therefore used in all subsequent transformations.

The 'directing' role of the *N*-pyrrole amide function is supported by the observation that none of the desired arylated products were observed when the 3- and 4-chloro-substituted substrates **7a** or **b** were used. In both cases none of the side-product **6** was observed, indicating that the competing hydrodehalogenation reaction is also a substrate-directed process.

Turning to the influence of different amide-based directing groups, *N*-indole amide proved to be less useful than the analogous *N*-pyrrole amide, giving the structurally characterised (Figure 2(c)) product **5b** in moderate yield. A modest amount of the product **5c** was also obtained using the *N*,*N*-diphenyl amide directing group. By contrast, little or none of the products **5d** - **g** was obtained from substrates with a variety of amide-based directing groups.

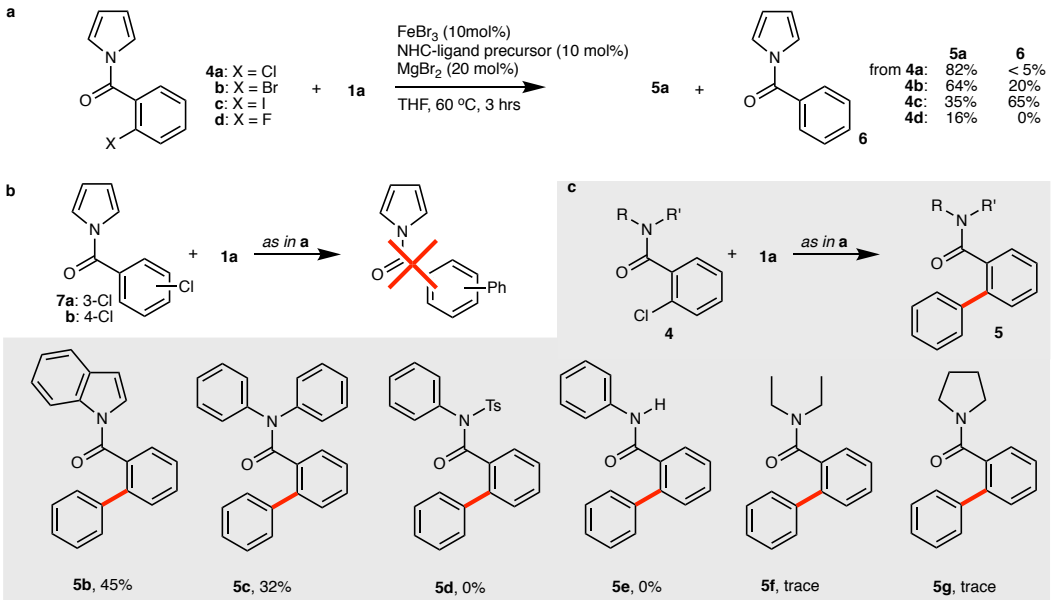

Figure 3. The influence on the reaction of type and position of the aryl halide. Varying **a**, the 2-halide, **b**, the position of chloride and **c**, the amide-based directing group. Spectroscopic yields, based on ^{1}H NMR spectroscopy (1,3,5-trimethoxybenzene internal standard), expect for **5f** and **5g** whose presence in low levels was detected by GC-MS.

Scope and limitations of the reaction.

With the optimised conditions in hand (Table 1, entry 14), we next explored the scope and limitations of the transformation, and these results are summarised in Table 2. Starting with the boronate **1a** and varying the substitution on the aryl chloride revealed that alkoxy (**5h** – **j**), alkyl (**5k** – **m**), nitrile (**5o**) and remote chloro (**5p**) functional groups could all be accommodated. The production of **5m** demonstrates that modest steric hindrance does not cause an issue, meanwhile the isolation of **5p** again lends strong support to the suggestion that C-Cl bond activation of the starting material is dependent on an *ortho*-directing group involvement. Disappointingly, the acetophenone moiety was not tolerated, with only trace amounts of **5n** observed.

Incorporating *para*-anisole into the boronate reagent gave coupling products with a range of electrophiles which included bromo (**5r**), fluoro (**5s** and **t**), trifluoromethyl (**5u**), tertiary amine (**5v**) and thioether (**5w**) moieties. Modest performance was also seen when the aryl chloride was replaced by a 2-chloropyridine-containing analogue (**5y**); unfortunately, when a heterocyclic (thiophene) boronate was used, none of the desired product (**5z**) was obtained. Moderate to good activity was observed with 4-tolyl, 2-naphthyl and 4-chlorophenyl derived boronates (products **5aa** – **5ac**).

Table 2. Scope and limitations of *N*-pyrrole amide-directed, iron-catalysed Suzuki biaryl coupling.

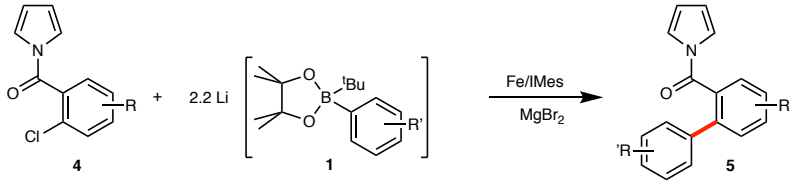

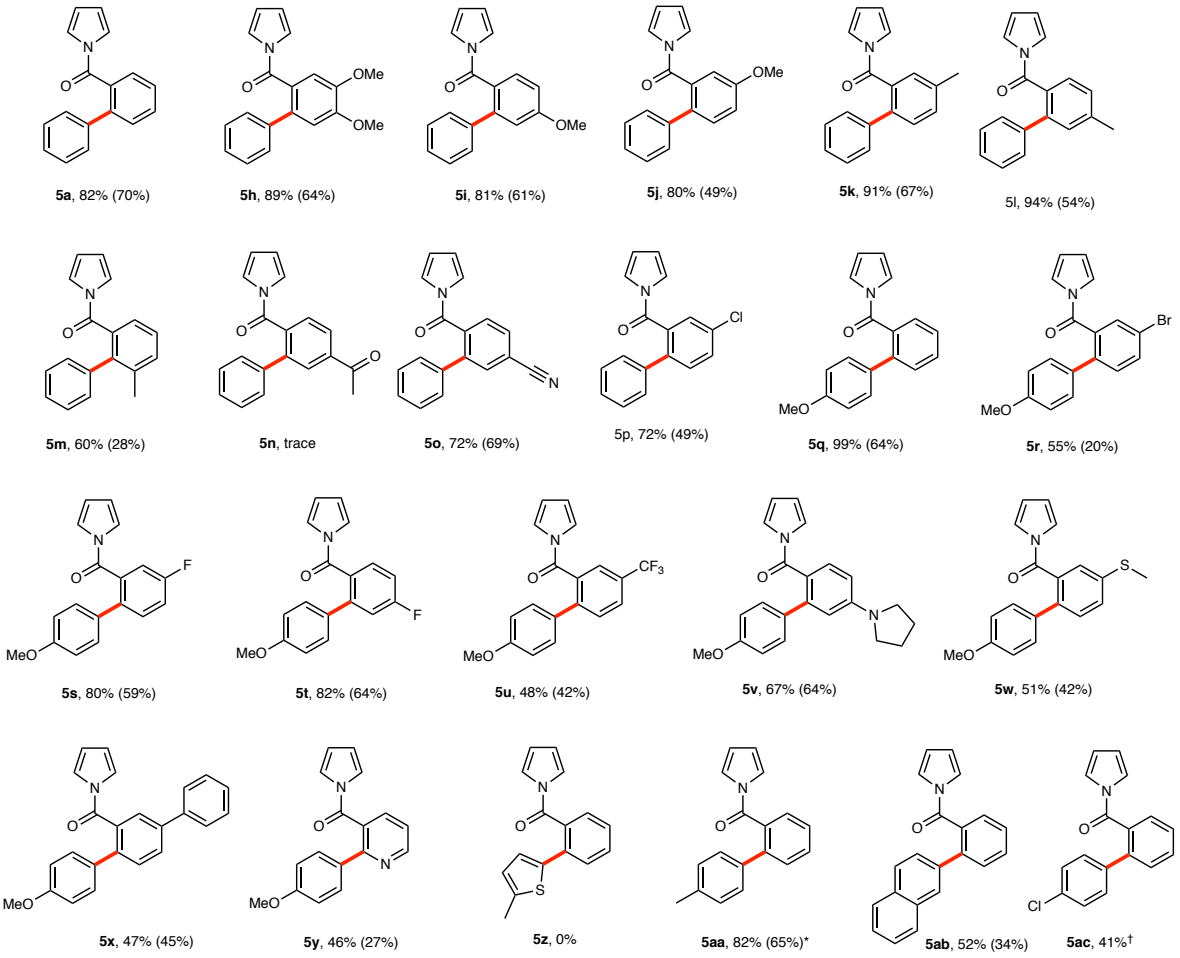

Spectroscopic yields, determined by ^{1}H NMR spectroscopy (1,3,5-trimethoxybenzene internal standard, except for **5ab**, where 3,4,5-trichloropyridine was used); isolated yields given in parentheses. *Boronate salt formed *in situ*. † **5ac** formed an inseparable mixture with residual aryl chloride starting material. See Methods and Supplementary Methods for full details and characterisation.

Mechanistic investigations.

We have undertaken a variety of mechanistic studies, the first of which was to establish the lowest thermodynamically viable oxidation state that can be accessed by iron under the reaction conditions, since Fe(0),[33-35], Fe(I)[36,37] and Fe(II)[38-40] complexes can all be supported by NHC ligands.[41] The boronate nucleophile acts as a reducing reagent for the iron; accordingly a mixture of $FeCl_2$ and **IMes** was reacted with **1a** and $MgBr_2$ in the presence of

divinyltetramethyldisiloxane (dvtms) as a trapping reagent. This led to the formation of the known iron(0) complex **8** (Figure 4(a)),[34] as characterised by paramagnetic proton NMR and X-ray crystallography (see Supplementary Methods and Supplementary Figures 2 and 16). The same result was obtained when $MgBr_2$ was omitted, using either **IMes** or **IMes·HCl** as the carbene source; the latter result clearly indicates that the borate **1a** is sufficiently basic to deprotonate the imidazolium in the presence of iron, while both results show that $MgBr_2$ is not required for the reduction. The zero-valent complex **8** proved to be a competent pre-catalyst in the coupling of **1a** with **4a**, giving **5a** in 73% spectroscopic yield after 3 hours (see Supplementary Methods). This data indicates that Fe(0) may be formed during the reaction, but it should be noted that by itself this does not rule out the possibility that the such Fe(0) species represent thermodynamically stable resting states rather than kinetically relevant catalytic intermediates: the lowest oxidation state of the species on the catalytic cycle may well be higher than, but not lower than, Fe(0).[42]

In the absence of the diene, dvtms, to trap zero-valent iron complexes it is conceivable that low-valent, low-coordinate intermediates undergo aggregation to form iron nanoparticles. Such nanoparticles have previously been shown to be catalytically competent in cross-coupling reactions,[43] although whether they are the active catalysts or rather a catalyst resting state is open to question. Indeed we have previously found that the iron nanoparticles readily dissolve in the presence of an excess of an electrophilic coupling partner.[44] During the first few seconds of the Suzuki reaction, the catalytic mixtures are colourless, followed by a rapid darkening, broadly coincident with the end of the induction period (*vide infra*). TEM analysis of a sample removed after 90 seconds in the coupling of **1a** with **4a** revealed a patchy network of deposited salts (Supplementary Figure 3). No obvious populations of electron-dense, iron-rich nanoparticles were discernible. EDX analysis indicated the deposits contained Mg, Br, Cl and Fe and elemental mapping confirmed all four of these elements were relatively homogeneously distributed throughout the structures (Supplementary Figure 4). Furthermore, a mercury drop experiment showed no significant impact on either the productivity of the catalytic reaction, or on the rate of catalysis (Supplementary Methods and Supplementary Figure 5). Meanwhile, the use of either pre-formed iron nanoparticles, supported by a polytheylene glycol stabiliser,[43] or a mixture of $FeBr_3$/polyethylene glycol as the pre-catalyst gave no better results than when $FeBr_3$ was used on its own (Supplementary

Methods and Supplementary Table 1). Taken together, these observations suggest that nanoparticles are unlikely to be the active catalysts. Furthermore, the strong ligand-dependence of the catalytic reaction lends credence to the suggestion that at least part of the cycle occurs in the homogeneous phase.

No cross-coupling was observed in the absence of $MgBr_2$. A brief survey of alternative bromide additives revealed that the coupling of **1a** with **4a** gave the product **5a** with varying degrees of success: $AlBr_3$ (76%), NaBr (40%), KBr (39%), $ZnBr_2$ (23%) LiBr (5%) and NBu_4Br (no reaction). The complete lack of activity in the latter case may be due to poor solubility of the salt under the reaction conditions. Meanwhile, the use of $MgCl_2$ in place of the bromide gave 84% of **5a**. It is tempting to conclude that with MgX_2, $AlBr_3$ or $ZnBr_2$ that organo-main group metal intermediates form and subsequently engage in transmetallation to the iron.[21,22] However, neither the Zn nor Al-based nucleophiles, $Ph_2Zn/MgBr_2$ or $MgBr[Al(4\text{-tolyl})_4]$, when used in place of **1a**, gave significant activity, even though these nucleophiles have previously been successfully exploited in iron-catalysed cross-couplings,[21,26,44-48] strongly suggesting that neither metal halide facilitates transmetallation. Meanwhile PhMgBr shows some activity, giving the product **5a** in 45% yield, however this is accompanied by very significant biphenyl production. Again this result is not consistent with the Mg aiding the transmetallation in the Suzuki reaction.

We next probed the effect of varying $MgBr_2$ loading on the rate of the reaction. Figures 4(b) and (c) show the formation of cross-coupled product, **5a**, and the side-product, biphenyl (**9**), against time in the coupling of **1a** and **4a** at various $MgBr_2$ loadings (see Supplementary Methods and Supplementary Figure 6 for full details). In all cases, a clear catalyst induction period of around 8 seconds was observed before maximal rate of formation of **5a** was achieved and this induction period corresponds to the production of the majority of the biphenyl (**9**) observed in the reactions. The formation of biphenyl from two equivalents of **1a** corresponds to the release of two electrons, which are used in the reduction of the iron. From the plateaued concentration of **9** after the induction period, it is possible to calculate that the average number of electrons liberated corresponds to around 0.75 per iron centre,[45] which may in turn correspond with reduction of the Fe(III) pre-catalyst to an average oxidation state for the bulk of the iron of approximately Fe(II). This suggests that while Fe(0) can be

thermodynamically accessed by the reductant **1a** (*vide supra*), kinetically, the lowest average oxidation state may be two units higher. Again, care must be taken here as the average oxidation state value may conceal, for example, disproportionation or comproportionation processes, either of which can yield a variety of different oxidation state species in the reaction mixture.[42] Irrespective of the precise mechanism of reduction of the iron pre-catalyst, it is clear that this process is not dependent on magnesium bromide, since the duration of the induction period is unperturbed by the $MgBr_2$ loading.

Figure 4(d) summarises the rate of cross-coupling at the various $MgBr_2$ loadings. It is apparent that there is a strong correlation between $MgBr_2$ loading and rate between 7.5 mol% and 20 mol%; below this range there was no activity, while above the reaction started to slow. Clearly, while the bromide is necessary for activity, above a certain point it plays an inhibitory role on the reaction, suggesting intervention at more than one point in the cycle. The data are also indicative of a change in the rate-determining process with increasing bromide concentration, and this was further supported by kinetic isotope effect (KIE) studies. These were performed at both 15 and 20 mol% $MgBr_2$ loadings (using **1d** as the nucleophile), employing a competition between deuterated and non-deuterated electrophiles (see Supplementary Methods and Supplementary Figures 7 - 10). At 20 mol% loading, no KIE was observed, but at 15 mol% - well within the region where a strong positive influence of $MgBr_2$ loading was observed – an inverse secondary KIE of 0.72 was obtained. This KIE is consistent with the involvement of π-coordination of the pyrrole in the rate-determining step or a pre-equilibrium with the rate-determining step, which would entail an increase in *p*-character in the hybridisation of the pyrrole's carbon atoms.[49] π-Coordination of pyrroles to iron is well known, with two examples of structurally characterised *N*-alkyl pyrrole iron(II) complexes reported previously.[50,51] In addition, η^5-*N*-acyl pyrrole complexes of Fe(II) have been reported, although not structurally characterised.[52,53]

To garner further information on the intervention of $MgBr_2$ in the catalytic cycle, we undertook kinetic analyses of the reactions between **1a** and **4a** run at both 15 and 25 mol% $MgBr_2$ loadings (see Supplementary Methods and Supplementary Figure 11 for details). The data obtained at 15 mol% $MgBr_2$ – the loading where we observed an inverse secondary kinetic isotope effect – revealed an approximately 0.8 order dependence on [IMes/Fe] up to

10 mol% Fe loading, beyond which the rate slowed, and an approximately 0.5 order dependence on [**4a**]. The rate showed an approximately 1st order dependence on the nucleophile up to around 2.5 equivalents, beyond which no dependence was observed. The data for the reactions performed at 25 mol% $MgBr_2$ – a loading beyond the point where no KIE was observed – show similar behaviour, with orders of approximately 0.7 for both [**4a**] and [Fe] respectively as well as an approximately first order dependence on the boronate nucleophile up to around 2.5 equivalents, with no dependence above this range.

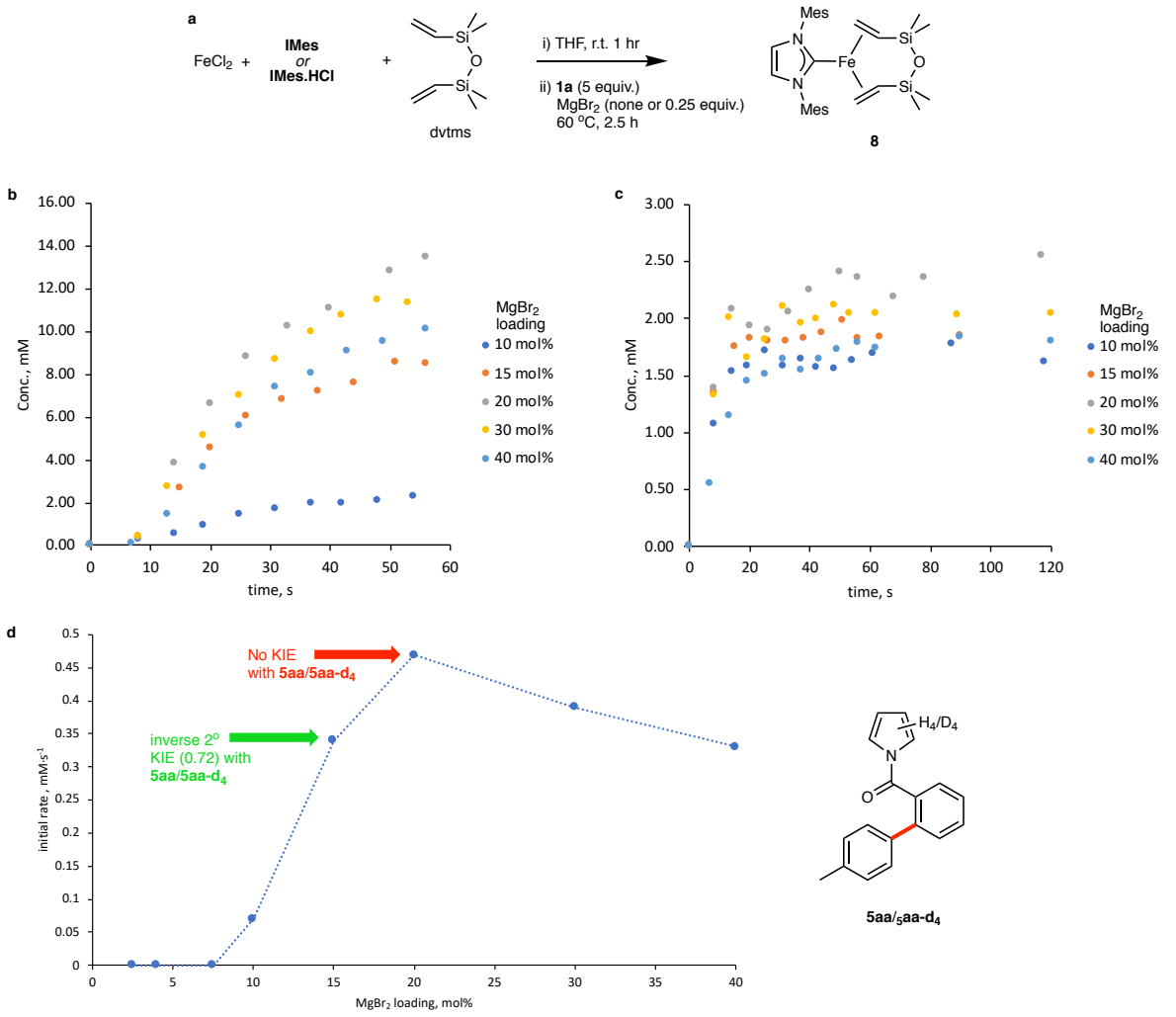

Figure 4. Mechanistic investigations. a, Model reduction reaction of Fe(II) to Fe(0) by the boronate **1**. **b** and **c** Formation against time of the cross-coupled product **5a** and the homocoupled side-product **9** against time respectively with varying (10 – 40 mol%) $MgBr_2$ loadings. **d**, Rates of cross-coupling with varying (2.5 – 40 mol%) $MgBr_2$ loadings and kinetic isotope effects (KIE) at 15 and 20 mol% loadings. The KIEs were determined by comparing relative amounts of **5aa**/**5aa-d$_4$** formed in the Suzuki coupling of **1d** (R' = 4-Me) with a 50:50 mixture of **4a**/**4a-d$_4$** (see Supplementary Methods for experimental details).

Figure 5 shows a tentative, simplified model for a catalytic cycle that is consistent with all the observations described above. The pre-catalyst, [pre-Fe], undergoes an activation process to generate the reduced active aryl complex, **A**, with concomitant liberation of biphenyl, a process that is independent of [$MgBr_2$]. We suggest that reversible pyrrole π-coordination of the substrate **4a** to **A** is followed by reversible coordination of "Br^-" (either bromide or a more complex adduct of $MgBr_2$), which is in turn followed by irreversible activation of **4a** to give the intermediate **D**. Note, **A**, **B** and **F** may instead be cationic intermediates, in which case **C** **D** and **E** would be neutral. Either way, the coordination of bromide to **B** would lead to an increases in electron-density on the iron centre of **C** which would in turn facilitate the subsequent C-Cl bond activation. The observation of a KIE at this magnesium salt loading indicates that the π-coordination of the pyrrole to **A** to give **B** is both reversible and faster than the conversion of **B** to **C**. In addition to the dependence of the rate on [$MgBr_2$], the proposed pre-equilibria can account for both the positive dependence of the rate on [Fe] and [**4a**] and the observed non-integer values.

As the concentration of $MgBr_2$ increases, the rate of conversion of **B** to **C** increases, until it is faster than the conversion of **A** to **B**, ultimately rendering the latter transformation essentially irreversible, at which point onwards no KIE is observed. Beyond 20 mol% loading of $MgBr_2$ the rate of catalysis slows with increasing concentration. In the proposed model, this is explained by the slowing down of the rate of the reversible loss of bromide/$MgBr_2$ from the intermediate **E** which in turn impacts directly upon the transmetallation step **F** → **A**. At the higher $MgBr_2$ loadings, the presence of the equilibria between **E**, **F**, **A**, **B** and **C** can account for the observed fractional order dependence of the rate on the concentrations of the electrophile, the nucleophile and the iron.

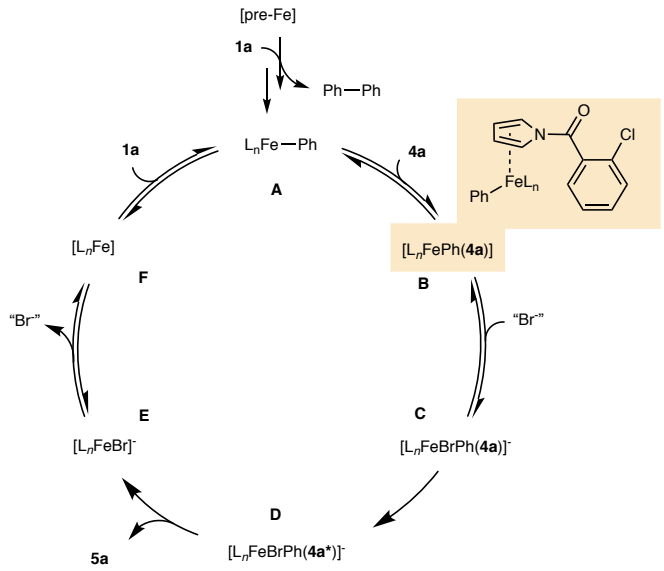

Figure 5. Tentative and simplified catalytic cycle. In intermediate **B**, **4a** interacts with the iron via pyrrole π-coordination (highlighted). In intermediate **D**, **4a*** represents the electrophilic substrate after activation of the C-Cl bond, most likely to give a σ-aryl-Fe complex. Throughout, "Br^-" may be bromide or $MgBr_2$, while Br in the formulae of intermediates may represent bromide or a more complex species such as an $MgBr_2$-Fe adduct. Anionic charges shown represent an increase in electron-density, not necessarily a formal negative charge: **C**, **D** and **E** may be neutral in which case **A**, **B** and **F** would be cationic.

A key feature of the suggested catalytic cycle is π-coordination of the pyrrole ligand which is proposed to help tether the substrate in the coordination sphere, facilitating the C-Cl bond activation. The observed KIE provides strong evidence in favour of π-coordination rather than coordination of the oxygen of the amide function, in isolation, being primarily responsible for the directing group effect. The pyrrole hydrogens are too far removed from the metal centre in the latter scenario to induce a significant KIE. In the case of formation of a modest amount of the *N*-diphenyl-amido product **5c**, it is likely that one of the *N*-phenyl groups acts at the π-coordinating directing group. Furthermore, the productivity of the coupling reactions fall sharply in the order **5a** > **5c** > **5g** from their respective aryl halide starting materials, **4a**, **e** and **f**, and yet the *O*-donor ability as judged by decreasing C-O bond strength (determined by I.R. spectroscopy) is **4f** > **4e** > **4a** (ν(CO): **4f**, 1629; **4e**, 1654 and **4a** 1697 cm^{-1}). Interestingly, the substrate **10** could be arylated to give **11**, albeit in very low yield, despite lacking an amide function (Figure 6(a)). Moreover, the dichloro-substrate **12** gave the expected mono-arylated product **13** in good yield. Only trace amounts of the diarylated product **14** and none of the indole-C-7 mono-arylated product **15** were observed, despite the fact that *N*-COR directing

groups can be used effectively to direct indole C-H bond-functionalisation to this position, with a variety of metals.[54]

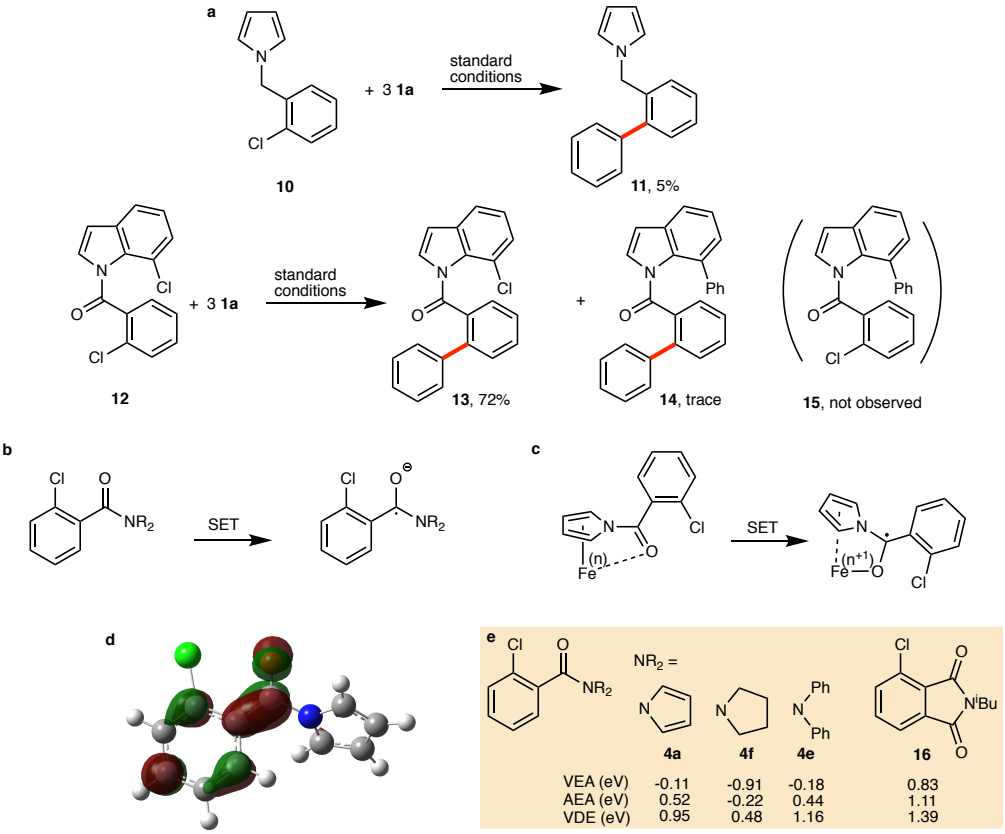

Figure 6. Probing pyrrole π-coordination and possible radical formation. a, Reactions to probe amide C=O directing ability. **b**, Formation of amino ketyl radicals and **c** possible involvement of carbonyl coordination in the reduction. **d**, Calculated (B3LYP/6-311G**) singly occupied frontier orbital (SOMO) for the amino ketyl radical **[4a]**$^{\cdot-}$, isovalue = 0.05 (electron/bohr^3)^{½}. **e**, Calculated gas phase vertical electron affinities (VEA), adiabatic electron affinities (AEA) and vertical detachment energies (VDE) (B3LYP/6-311G**).

In the proposed catalytic cycle above, intermediate **D** is most likely a σ-aryl iron complex formed by C-Cl bond cleavage, but at this stage we cannot rule out the possibility that it may instead consist of a 'trapped' radical. Either way, it is quite possible that the C-Cl cleavage proceeds via single-electron transfer (SET) rather than classical oxidative addition, as has been observed previously with cobalt.[55] Indeed, the use of the radical-trap TEMPO led to inhibition of the coupling reaction (see Supplementary Methods for details). By contrast, the use of styrene as a potential arylboronate radical scavenger,[56] had essentially no impact on productivity (Supplementary Methods).

As well as playing a directing role, the *N*-pyrrole amide group may electronically activate the substrate with respect to oxidative C-Cl bond-scission *via* the formation an intermediate amino ketyl radical (Figure 6(b)),[57] perhaps following coordination of the C=O function to the iron centre (Figure 6(c)). While some caution must be exercised in the use of computed thermodynamic metrics for processes that proceed *via* one or more unverified transitions states, by invoking the Hammond postulate it should, in principle at least, be possible to rank the observed relative reactivity with the calculated stability of the radical anions. A density functional theory examination (see Supplementary Methods for full details) of the amino ketyl radicals formed from the substrates **4a**, **e** and **f** revealed very similar frontier orbitals in each case, with the unpaired electron delocalised across both the ketyl function and the in-plane aryl chloride, with essentially no contribution from the out-of-plane NR_2 group. One example, **[4a]**$^{\cdot-}$, the radical formed from **4a**, is shown in Figure 6(d), while the others are given in Supplementary Figure 12. An examination of the vertical electron affinity (VEA) and the adiabatic electron affinity (AEA) for the substrates **4a**,**e** and **f** (Figure 6(e)) and the vertical detachment energy (VDE) of the associated radical anions (see Supplementary Methods for full details, further discussion and Supplementary Table 2 for solution-phase values) revealed that the order of increasing electron affinity of the substrates matched the order of productivity in the reactions, consistent with the intermediacy of a ketyl radical. Importantly, we were able to use the calculated trends to predict that the phthalimide-based substrate **16** should undergo significantly more facile single-electron reduction than even substrate **4a**. While **16** has a carbonyl group that can direct the C-Cl bond cleavage, it lacks an appropriate π-coordinating directing group. A catalytic reaction between **16** and **1a** not only appeared strikingly different, with a deep blue colouration apparent after the first few seconds, but also gave none of the desired cross-coupled product, despite the propensity of **16** to form an amino ketyl radical. None of the starting material **16** was recovered, however 26% of the hydrodehalogenated material, *N*-isobutyl phthalimide, was obtained. It is apparent that the ability to form a ketyl radical, coupled with the presence of an amido group *ortho* to the aryl chloride residue is not sufficient for activity, in the absence of a π-coordinating directing group, even when an electronically-activated substrate is employed.

Conclusions.

In summary, we have demonstrated that iron-catalysed Suzuki biaryl cross-coupling is an achievable goal. Currently the reaction is reliant on the use of π-coordinating pyrrole and related directing groups to direct C-X bond activation, but once this occurs, all of other steps are viable. Critically, the work reported here indicates that in order to realise routine, general iron-catalysed Suzuki biaryl cross-coupling, future endeavours should focus on optimising catalyst structure to facilitate non-directed aryl-halide bond activation.

Methods.

General procedure for the preparation of *N*-pyrrole amides, 4. Starting from the appropriate halobenzoic acid; all reactions performed under nitrogen atmosphere, whilst extraction and purification were performed under aerobic conditions. To a 100 ml round-bottom flask was added the appropriate halobenzoic acid (5.5 mmol), CH_2Cl_2 (20 ml) and DMF (5 drops). Thionyl chloride (4.01 ml, 55 mmol) was added slowly and the solution stirred for 2 h at room temperature. The solvent and excess thionyl chloride were then removed *in vacuo,* and the crude halobenzoic acid chloride obtained was dissolved in THF (20 ml). In a separate 100 ml round-bottom flask pyrrole (0.347 ml, 5 mmol) was dissolved in THF (20 ml), the solution cooled to 0 °C and sodium hydride (60 % dispersion in mineral oil, 200 mg, 5 mmol) was added in one portion. The mixture was stirred for 30 min at 0 °C, during which time effervescence was observed, and then warmed to room temperature and stirred for a further 30 min. The mixture was then cooled to 0 °C and the crude halobenzoic acid chloride solution (above) was added *via* cannula. The reaction mixture was warmed to room temperature, stirred overnight and then quenched by the addition of 1 M HCl (10 ml). The organics were extracted from the aqueous layer with CH_2Cl_2 (3 x 15 ml), combined, dried over $MgSO_4$, filtered and the solvent removed under reduced pressure to afford the crude product **4** which was purified by flash column chromatography. Alternatively, where the halobenzoic acid chloride was commercially available, the material was added in a single portion directly to the deprotonated pyrrole solution.

General procedure for the iron-catalysed directed Suzuki biaryl cross-coupling reaction. Under an atmosphere of nitrogen, in a dry Schlenk tube, IMes·HCl (13.6 mg, 0.04 mmol) was stirred with a solution of $FeBr_3$ (0.02 M in THF, 2 ml, 0.04 mmol) at room temperature for 1

h. To this solution was added sequentially a solution of $MgBr_2$ (0.1 M in THF, 0.8 ml, 0.08 mmol), the appropriate halobenzamide substrate **4** (0.4 mmol) and the appropriate activated boronate **1** (0.4 M in THF, 2.2 ml, 0.88 mmol). The reaction was stirred for 2-3 h at 60 °C and then quenched by the addition of 1 M HCl (10 ml). The organics were extracted from the aqueous layer with CH_2Cl_2 (3 x 10 ml), the combined organics layers dried over $MgSO_4$ and filtered. 1,3,5-Trimethoxybenzene (internal standard, 67.3 mg, 0.4 mmol) was added and an aliquot taken for analysis by ^1H NMR spectroscopy. The crude mixture was then purified by flash column chromatography (and where necessary preparative thin-layer chromatography) to yield the desired cross-coupled biaryl product, **5**.

Acknowledgements

We thank the EPSRC for funding (Grant no. EP/K012258/1); for the provision of a studentship through the EPSRC Centre for Doctoral Training in Catalysis (M.M.) and for a part-studentship (H.M.O'B.). We thank AstraZeneca for CASE top-up funding (H.M.O'B.) and Andrew Stark (AZ) and Dr Natalie Fey for informative and useful discussions.

Author contributions

H.M.O'B., M.M., R.D.A., R.B.B. D.E., H.A.S. and S.A.D. performed and analysed experiments. H.M.O'B., R.D.A. and R.B.B. designed optimisation experiments. H.M.O.'B., M.M. and R.B.B. designed experiments to study effect of varying halide and directing groups. H.M.O'B. and R.B.B. designed experiments to explore scope of the reaction. H.M.O'B., M.M. and R.B.B. designed experiments to probe the mechanism. R.B.B. designed computational experiments. H.M.O'B., M.M. and R.B.B. prepared this manuscript.

Additional information

Detailed experimental methods and compound characterisation data are provided online in the Supplementary Information. Correspondence and requests for materials should be addressed to R.B.B.

Competing interests

The authors declare no competing interests.

Data availability:

Crystal structure data for **1a**, **5a**, **5b** and **8** have been deposited at the Cambridge Crystallographic Data Centre (CCDC nos: 1587839-1587842 respectively) and crystallographic data are provided in the Supplementary Information. The spectroscopic, mass spectrometric, TEM and kinetic data that support the findings of this study are freely available in the University of Bristol data repository, data.bris, with the identifier DOI: 10.5523/bris.1egk09qs16sej2ru76yju7q572

References

1. Miyaura, N. & Suzuki A. Palladium-Catalyzed Cross-Coupling Reactions of Organoboron Compounds. *Chem. Rev.* **95**, 2457-2483 (1995).

2. Valente, C. & Organ M. G. The Contemporary Suzuki–Miyaura Reaction, in *Boronic Acids* pp 213 – 262. (Ed.: D. G. Hall, Wiley, Weinheim, 2011).

3. Torborg, C., Beller, M. Recent Applications of Palladium-Catalyzed Coupling Reactions in the Pharmaceutical, Agrochemical, and Fine Chemical Industries. *Adv. Synth. Catal.* **351**, 3027-3043 (2009).

4. Garrett, C. E. & Prasad, K. The Art of Meeting Palladium Specifications in Active Pharmaceutical Ingredients Produced by Pd-Catalyzed Reactions. *Adv. Synth. Catal.* **346**, 889-900 (2004).

5. Han, F.-S. Transition-metal-catalyzed Suzuki–Miyaura cross-coupling reactions: a remarkable advance from palladium to nickel catalysts. *Chem. Soc. Rev.* **42**, 5270-5298 (2013).

6. Mastalir, M., Stöger, B., Pittenauer, E., Allmaier, G. & Kirchner, K. Air-Stable Triazine-Based Ni(II) PNP Pincer Complexes As Catalysts for the Suzuki−Miyaura Cross-Coupling. *Org. Lett.*, **18**, 3186-3189 (2016).

7. Zhou, J., Berthel, J. H. J., Kuntze-Fechner, M. W., Friedrich, A.; Marder, T. B. & Radius, U. NHC Nickel-Catalyzed Suzuki−Miyaura Cross-Coupling Reactions of Aryl Boronate Esters with Perfluorobenzenes. *J. Org. Chem.*, **81**, 5789-5794 (2016).

8. Shi, S., Meng, G. & Szostak, M. Synthesis of Biaryls through Nickel-Catalyzed Suzuki–Miyaura Coupling of Amides by Carbon–Nitrogen Bond Cleavage*. Angew. Chem. Int. Ed.* **55**, 6959-6963 (2016).

9. Malan, F. P., Singleton, E., van Rooyen, P. H. & Landman. M. Facile Suzuki-Miyaura coupling of activated aryl halides using new CpNiBr(NHC) complexes. *J. Organomet. Chem.*, **813**, 7-14 (2016).

10. Shields, J. D., Gray, E. E. & Doyle, A. G. A Modular, Air-Stable Nickel Precatalyst. *Org. Lett.*, **17**, 2166-2169 (2015).

11. Thapa, S. Shrestha, B. Gurung, S. K. & Giri, R. Copper-catalysed cross-coupling: an untapped potential. *Org. Biomol. Chem.* **13**, 4816-4827 (2015).

12. Gurung, S. K. Thapa, S., Shrestha, B. & Giri, R. Copper-catalysed cross-couplings of arylboronate esters with aryl and heteroaryl iodides and bromides. *Org. Chem. Front.*, **2**, 649−653 (2015).

13. Zhou, Y., You, W., Smith, K. B. & Brown, M. K. Copper-Catalyzed Cross-Coupling of Boronic Esters with Aryl Iodides and Application to the Carboboration of Alkynes and Allenes. *Angew. Chem. Int. Ed.*, **53**, 3475−3479 (2014).

14. Gurung, S. K., Thapa, S., Kafle, A., Dickie, D. A. & Giri, R. Copper-Catalyzed Suzuki−Miyaura Coupling of Arylboronate Esters: Transmetalation with (PN)CuF and Identification of Intermediates. *Org. Lett.*, **16**, 1264−1267 (2014).

15. Neely, J. M., Bezdek, M. J. & Chirik P.J. Insight into Transmetalation Enables Cobalt-Catalyzed Suzuki− Miyaura Cross Coupling. *ACS Cent. Sci.*, **2**, 935-942 (2016).

16. Asghar, S., Tailor, S. B., Elorriaga D. & Bedford, R. B. Cobalt-catalyzed Suzuki biaryl coupling of aryl halides. *Angew. Chem. Int. Ed.* **56**, 16367–16370 (2017).

17. Duong, H. A.; Wu, W. & Teo, Y.-Y. Cobalt-Catalyzed Cross-Coupling Reactions of Arylboronic Esters and Aryl Halides. *Organometallics* 10.1021/acs.organomet.7b00726

18. Nakamura, E., Hatakeyama, T., Ito, S., Ishizuka, K., Ilies, L. & Nakamura, M. Iron-Catalyzed Cross-Coupling Reactions, *Org. React.*, **83**, 1-210 (2014)

19. Bedford, R. B. & Brenner, P. B. The Development of Iron Catalysts for Cross-Coupling Reactions. *Top. Organomet. Chem*., **50**, 19-46 (2015)

20. Bauer, I. & Knölker, H.-J. Iron Catalysis in Organic Synthesis. *Chem. Rev.*, **115**, 3170–3387 (2015).

21. Bedford, R. B., Hall, M. A., Hodges, G. R., Huwe, M. & Wilkinson. M. C. Simple mixed Fe–Zn catalysts for the Suzuki couplings of tetraarylborates with benzyl halides and 2-halopyridines *Chem. Commun.*, 6430-6432 (2009).

22. Hatakeyama, T., Hashimoto, T., Kondo, Y., Fujiwara, Y., Seike, H., Takaya, H., Tamada, Y., Ono, T. & Nakamura, M. Iron-Catalyzed Suzuki−Miyaura Coupling of Alkyl Halides. *J. Am. Chem. Soc.*, **132**, 10674-10676 (2010).

23. Hashimoto, T., Hatakeyama, T. & Nakamura, M. Stereospecific Cross-Coupling between Alkenylboronates and Alkyl Halides Catalyzed by Iron–Bisphosphine Complexes. *J. Org. Chem.* **77**, 1168-1173 (2012).

24. Hatakeyama, T., Hashimoto, T., Kathriarachchi, K. K. A. D. S., Zenmyo, T., Seike, H. & Nakamura, M. Iron-Catalyzed Alkyl–Alkyl Suzuki–Miyaura Coupling. *Angew. Chem., Int. Ed.*, *51*, 8834-8837 (2012).

25. Bedford, R. B., Brenner, P. B., Carter, E., Carvell, T. W., Cogswell, P. M., Gallagher, T., Harvey, J. N., Murphy, D. M., Neeve, E. C., Nunn, J. & Pye, D. R. Expedient Iron-Catalyzed Coupling of Alkyl, Benzyl and Allyl Halides with Arylboronic Esters. *Chem. Eur. J.*, **20**, 7935-7938, (2014).

26. Bedford, R. B., Brenner, P. B., Carter, E., Clifton, J., Cogswell, P. M., Gower, N. J., Haddow, M. F., Harvey, J. N., Kehl, J. A., Murphy, D. M., Neeve, E. C., Neidig, M. L., Nunn, J., Snyder, B. E. R. & Taylor, J. Iron Phosphine Catalyzed Cross-Coupling of Tetraorganoborates and Related Group 13 Nucleophiles with Alkyl Halides. *Organometallics*, **33**, 5767-5780 (2014).

27. Bedford, R. B., Nakamura, M., Gower, N. J., Haddow, M. F., Hall, M. A., Huwe, M., Hashimoto, T. & Okopie R. A. Iron-catalysed Suzuki coupling? A cautionary tale. *Tetrahedron Lett.* **50** 6110–6111 (2009).

28. Kylmälä, T., Valkonen, A., Rissanen, K., Xu, Y. & Franzén, R. trans-Tetrakis(pyridine)dichloroiron(II) as catalyst for Suzuki cross-coupling in ethanol and water *Tetrahedron Lett.*, **49**, 6679-6681 (2008)

29. Beźier, D. & Darcel, C. Iron-Catalyzed Suzuki–Miyaura Cross-Coupling Reaction. *Adv. Synth. Catal.,* **351**, 1732−1736 (2009).

30. Guo, Y., Young, D. J. & Hor, T. S. A. Palladium-free Suzuki–Miyaura cross-coupling at elevated pressures. *Tetrahedron Lett.*, **49**, 5620-5621 (2008).

31. Bedford, R. B., Gallagher, T., Pye, D. R. & Savage, W. Towards Iron-Catalysed Suzuki Biaryl Cross-Coupling: Unusual Reactivity of 2-Halobenzyl Halides. *Synthesis*, **47**, 1761-1765 (2015).

32. Gülak, S., Gieshoff, T. N. & Jacobi von Wangelin, A. Olefin-Assisted Iron-Catalyzed Alkylation of Aryl Chlorides. *Adv. Synth. Catal.*, **355**, 2197-2202 (2013).

33. Blom, B., Tan, G., Enthaler, S., Inoue, S., Epping, J. D. & Driess, M. Bis-N-Heterocyclic Carbene (NHC) Stabilized η^6-Arene Iron(0) Complexes: Synthesis, Structure, Reactivity, and Catalytic Activity. *J. Am. Chem. Soc.*, **135**, 18108−18120 (2013).

34. Zhang, H., Ouyang, Z., Liu, Y., Zhang, Q., Wang, L. & Deng, L. (Aminocarbene)(Divinyltetramethyldisiloxane)Iron(0) Compounds: A Class of Low-Coordinate Iron(0) Reagents. *Angew. Chem. Int. Ed.*, **53**, 8432-8426 (2014).

35. Hashimoto, T., Hoshino, R., Hatanaka, T., Ohki, Y. & Tatsumi, K. Dinuclear Iron(0) Complexes of N-Heterocyclic Carbenes. *Organometallics*, **33**, 921−929 (2014).

36. Mo, Z., Ouyang, Z., Wang, L., Fillman, K. L., Neidig, M. L. & Deng, L. Two- and three-coordinate formal iron(I) compounds featuring monodentate aminocarbene ligands. *Org. Chem. Front.,* **1**, 1040-1044 (2014).

37. Ouyang, Z., Du, J. Wang, L., Kneebone, J. L., Neidig, M. L. & Deng, L. Linear and T-Shaped Iron(I) Complexes Supported by N-Heterocyclic Carbene Ligands: Synthesis and Structure Characterization. *Inorg. Chem.*, **54**, 8808-8816 (2015).

38. Przyojski, J. A., Arman, H. D. & Tonzetich, Z. J. Complexes of Iron(II) and Iron(III) Containing Aryl-Substituted N-Heterocyclic Carbene Ligands. *Organometallics* **31**, 3264−3271 (2012).

39. Danopoulos, A. A. Braunstein, P., Wesolek, M., Monakhov, K. Y. Rabu, P. & Robert, V. Three-Coordinate Iron(II) N-Heterocyclic Carbene Alkyl Complexes. *Organometallics*, **31**, 4102–4105 (2012).

40. Dunsford, J. J., Evans, D. J., Pugh, T., Shah, S. N., Chilton, N. F. & Ingleson, M. J. Three-Coordinate Iron(II) Expanded Ring N-Heterocyclic Carbene Complexes. *Organometallics*, **35**, 1098–1106 (2016).

41. Ingleson, M. J. & Layfield, R. A. N-Heterocyclic carbene chemistry of iron: fundamentals and applications. *Chem. Commun.*, **48**, 3579–3589 (2012).

42. Bedford, R. B. How Low Does Iron Go? Chasing the Active Species in Fe-Catalyzed Cross-Coupling Reactions. *Acc. Chem. Res.*, **48**, 1485−1493 (2015).

43. Bedford, R. B., Betham, M., Bruce, D. W., Davis, S. A., Frost, R. M. & Hird, M. Iron nanoparticles in the coupling of alkyl halides with aryl Grignard reagents. *Chem. Commun.*, 1398–1400 (2006).

44. Bedford, R. B., Brenner, P. B., Carter, E., Cogswell, P. M., Haddow, M. F., Harvey, J. N., Murphy, D. M., Nunn, J. & Woodall, C. H. TMEDA in Iron-Catalyzed Kumada Coupling: Amine

Adduct versus Homoleptic “ate” Complex Formation. *Angew. Chem. Int. Ed.*, **53**, 1804 –1808 (2014).

45. Adams, C. J., Bedford, R. B., Carter, E. Gower, N. J., Haddow, M. F. Harvey, J. N. Huwe, M., Cartes, M. Á., Mansell, S. M., Mendoza, C., Murphy, D. M. Neeve, E. C. & Nunn, J. Iron(I) in Negishi Cross-Coupling Reactions. *J. Am. Chem. Soc.*, **134**, 10333−10336 (2012).

46. Bedford, R. B. Huwe, M. & Wilkinson, M. C. Iron-catalysed Negishi coupling of benzyl halides and phosphates, Chem. Commun., 600–602 (2009).

47. Kawamura, S., Ishizuka, K., Takaya, H., Nakamura, M. The first iron-catalysed aluminium-variant Negishi coupling: critical effect of co-existing salts on the dynamic equilibrium of arylaluminium species and their reactivity. *Chem. Commun.*, 6054-6056 (2010).

48. Bedford, R. B., Carter, E., Cogswell, P. M., Gower, N. J., Haddow, M. F., Harvey, J. N., Murphy, D. M., Neeve, E. C. & Nunn, J. Simplifying Iron–Phosphine Catalysts for Cross-Coupling Reactions. *Angew. Chem. Int. Ed.*, **52**, 1285 –1288 (2013).

49. Gómez-Gallego, M. & Sierra, M. A. Kinetic Isotope Effects in the Study of Organometallic Reaction Mechanisms. *Chem. Rev.*, **111**, 4857–4963 (2011).

50. Kuhn, N., Horn, E.-M., Zauder, E., Blaser, D. & Boese, R. Stable Sandwich Complexes with Pentamethylpyrrole Ligands. *Angew. Chem. Int. Ed. Engl.* **27**, 579-580 (1988)

51. Kowalski, K., Suwaki, N., Zakrzewski, J., White, A. J. P, Long, N. J. & Mann, D. J., In vitro DNA scission activity of heterometallocenes. *Dalton Trans.*, 743–748 (2007).

52. Kuhn, N., Schulten, M., Zauder, E., Augart, N. & Boese, R. Heterocycles as ligands. V. Synthesis and characterization of 2,3,4,5-tetramethyl-1-azaferrocene. *Chem. Ber.*, **122**, 1891-1896 (1989).

53. Kuhn, N., Kuhn, A. & Lampe, E.-M. Heterocycles as ligands. XI. Octamethyl-1,1'-diazaferrocene as a bifunctional nitrogen base. *Chem. Ber.*, **124**, 997-1002 (1991).

54. Leitch, J. A., Bhonoah, Y. & Frost, C. G. Beyond C2 and C3: Transition-Metal-Catalyzed C−H Functionalization of Indole. *ACS Catal.*, **7**, 5618−5627 (2017).

55. Zhu, D. & Budzelaar, P. H. M. Binuclear Oxidative Addition of Aryl Halides. *Organometallics*, **29**, 5759-5761 (2010).

56. Sandford, C. Rasappan, R. & Aggarwal, V. K. Synthesis of Enantioenriched Alkylfluorides by the Fluorination of Boronate Complexes. *J. Am. Chem. Soc.*, **137**, 10100−10103 (2015).

57. Shi, S. & Szostak, M. Aminoketyl Radicals in Organic Synthesis: Stereoselective Cyclization of Five- and Six-Membered Cyclic Imides to 2-Azabicycles Using SmI_2–H_2O. *Org. Lett.*, **17**, 5144−5147 (2015).